Theor Chem Acc (1999) 102:226–236
DOI 10.1007/s002149800m97

Theoretical
Chemistry Accounts

Regular article

Theoretical studies of the potential energy surface and wavepacket dynamics of the Li_3 system*

Masahiro Ehara[1], **Koichi Yamashita**[2]

[1]Department of Synthetic Chemistry and Biological Chemistry, Faculty of Engineering, Kyoto University, Kyoto 606-8501, Japan
[2]Department of Chemical System Engineering, Graduate School of Engineering, The University of Tokyo, Tokyo 113-8656, Japan

Received: 2 July 1998 / Accepted: 3 September 1998 / Published online: 8 February 1999

Abstract. The three-dimensional (3D) potential energy surface of the ground state of Li_3 was determined by the multireference configuration interaction method. The vibrational motions and pseudorotation were investigated by a 3D time-dependent wavepacket formalism. The analytical expression of the 3D surface is given and the results of vibrational analyses at several critical points are presented. The low-lying excited states of Li_3 were examined for the C_{2v} structure and the vertical and adiabatic excitation energies were calculated. The ground and singlet excited states of Li_2 were calculated and their spectroscopic constants compare well with the experimental values. A 3D wavepacket calculation was performed for simulations of the stimulated emission pumping spectrum in which the A state was taken as an intermediate. The recurrences of the autocorrelation functions were characterized by classical trajectory calculations. The autocorrelation functions obtained by wavepacket propagation are reproduced well by the accumulation of the classical trajectories in the short-time region.

Key words: Li_3 – Pseudorotations – Wavepacket dynamics – Potential energy surfaces

1 Introduction

Alkali trimers provide information on fundamental aspects of molecular spectroscopy such as pseudorotations and vibronic interactions. In such systems, there are some characteristic geometries, such as three-fold symmetric wells (C_{2v} obtuse), pseudorotation barriers (C_{2v} acute), and a D_{3h} Jahn-Teller crossing, which make the potential energy surface (PES) strongly anharmonic.

Delacretaz et al [1] have assigned the B state of Na_3 to $2^2E'$ and interpreted their spectrum in terms of a Jahn-Teller model. Ab initio calculations by Cocchini et al. [2] later predicted an additional, nondegenerate electronic state of $^2A_1'$ symmetry lying closely under the $^2E'$ state. Subsequently, Meiswinkel and Köppel [3] explained theoretically the spectrum based on a pseudo Jahn-Teller model. A congested stimulated emission pumping (SEP) spectrum was observed on a chaotic background for Na_3 by Broyer et al [4] and the vibrational motion in the chaotic region was then investigated theoretically and assigned based on unstable periodic orbits [5, 6]. Recently, continuous wave two-photon ionization and fs pump-probe spectroscopy [7, 8] have yielded preferential excitations of the pseudorotations and the symmetric stretch in $Na_3(B)$, respectively. The experimental results have been verified theoretically by using time-dependent wavepacket calculations [9–11].

The PES of Li_3 also has the characteristics seen for other alkali trimers, and the pseudorotation barrier is even lower than that of Na_3. The lowest adiabatic surface and the vibronic states of Li_3 were studied by Gerber and Schumacher [12] using the coupled electron pair approximation (CEPA). Martins et al [13] also calculated the lowest adiabatic surface by the pseudopotential and the local-spin-density approximation and Thompson et al fitted the surface with a well-designed analytical function [14]. Although Beckmann [15] calculated the vertical excitation energies for eight low-lying excited states of Li_3 by MRD-CI and the excitation to the $2^2E'$ state of Li_3 was first observed experimentally by Wolf et al [16], little is known about the excited states of Li_3.

In our study, the ground and excited electronic states of Li_3 and the vibrational motion and pseudorotation in the ground state were investigated. The three-dimensional (3D) PESs of the first and second adiabatic states were calculated by the multireference CI (MRCI) method with the state-averaged complete-active-space self-consistent field (CASSCF) reference. The lower PES was fitted by a consistent analytical function [14]. Twelve low-lying electronic states of Li_3 were investigated for the C_{2v} structure and the stable geometries were determined. The molecular dynamics were investigated by a 3D time-dependent wavepacket formalism to simulate a stimulated emission pumping (SEP) spectrum. The

* Contribution to the Kenichi Fukui Memorial Issue

Correspondence to: K. Yamashita

autocorrelation functions were calculated to find the recurrences and the origin of the recurrences was characterized by classical mechanics.

2 Calculational details

We calculated the ground and low-lying excited states of Li_2 and Li_3 by the MRCI method with the CASSCF [17] reference. All calculations were performed by the MOLPRO suite of ab initio programs [18].

The 3D PESs of the ground and first excited states of Li_3 conically intersect in a D_{3h} structure. The CASSCF calculations were performed by distributing three electrons into twelve orbitals, which correspond to all the Li $2s$ and $2p$ valence orbitals. In the MRCI, nine a' and three a'' MOs were adopted as active orbitals, and all single and double excitations into the external orbitals relative to the full CASSCF reference were taken into account. The correlation-consistent basis set of Dunning, VTZP(*spdf*)[4*s*3*p*2*d*1*f*] [19], was used for Li. Calculations were performed in the point group C_s and this yielded 321 and 41,172 configuration state functions in the CASSCF and MRCI calculations, respectively, for A' symmetry.

The ground and 11 low-lying valence excited states were also investigated by the CASSCF/MRCI method in the C_{2v} structure and the 2D PESs were obtained. All 12 electronic states were averaged with equal weight in the CASSCF calculations. The VTZP(*spd*) [4*s*3*p*2*d*] set [19] was adopted for Li. Resulting CSFs were about 160 and 11,000 for the CASSCF and MRCI calculations, respectively, for each irreducible symmetry. The 2D PESs for five $^2A_1$, four $^2B_1$, two $^2B_2$, and one $^2A_2$ states were calculated.

The ground and low-lying singlet excited states of Li_2 were also calculated for the fitting of the two-body terms of the Li_3 analytical potential function. The MRCI calculations were performed with the VDZP [3*s*2*p*1*d*], VTZP(*spd*) [4*s*3*p*2*d*], and VTZP(*spdf*) [4*s*3*p*2*d*1*f*] basis sets of Dunning [19].

We need to review the coordinate systems used in this work. Different coordinates are used for different purposes. The D_{3h} symmetry coordinates (q_s, q_x, q_y), that is, the normal coordinates of D_{3h}, are defined in relation to the Cartesian coordinates (x_i, y_i, z_i) of the three atoms by

$$q_s = -\frac{1}{2\sqrt{3}}x_1 - \frac{1}{6}y_1 + \frac{1}{2\sqrt{3}}x_2 - \frac{1}{6}y_2 + \frac{1}{3}y_3 \ , \tag{1}$$

$$q_x = \frac{1}{2\sqrt{3}}x_1 - \frac{1}{6}y_1 - \frac{1}{2\sqrt{3}}x_2 - \frac{1}{6}y_2 + \frac{1}{3}y_3 \ , \tag{2}$$

$$q_y = -\frac{1}{6}x_1 - \frac{1}{2\sqrt{3}}y_1 - \frac{1}{6}x_2 + \frac{1}{2\sqrt{3}}y_2 + \frac{1}{3}x_3 \ . \tag{3}$$

It is possible to describe any structure of the trimer molecule with these coordinates [12–14]. The relationships between these D_{3h} coordinates and the internuclear distances (r_{12}, r_{23}, r_{31}) are given by

$$\delta = \left(r_{12}^2 + r_{23}^2 + r_{31}^2\right) = 9\left(q_s^2 + q_x^2 + q_y^2\right) \ , \tag{4}$$

$$\beta = \sqrt{3}\left(r_{12}^2 - r_{31}^2\right) = -9q_s\left(\sqrt{3}q_x + q_y\right) \ , \tag{5}$$

$$\gamma = \left(2r_{23}^2 - r_{12}^2 - r_{31}^2\right) = 9q_s\left(q_x - \sqrt{3}q_y\right) \ . \tag{6}$$

Then, the hyperspherical coordinates (ρ, s, ϕ) are defined as

$$\rho = \left(r_{12}^2 + r_{23}^2 + r_{31}^2\right)/3 = \left(q_s^2 + q_x^2 + q_y^2\right)^{1/2} \ , \tag{7}$$

$$s = \sqrt{\beta^2 + \gamma^2}\Big/\delta = 2q_s\sqrt{q_x^2 + q_y^2}\Big/\left(q_s^2 + q_x^2 + q_y^2\right) \ , \tag{8}$$

$$\phi = \arctan\left(q_y/q_x\right) \ . \tag{9}$$

Note that the scales of our coordinates are exactly the same as those of Gerber and Schumacher [12], but differ from those of Thompson et al [14] by a factor of $\frac{1}{\sqrt{3}}$ for q_s, q_x, q_y, and ρ.

The lowest 3D PES is fitted with the analytical function expanded in hyperspherical coordinates. The functional form adopted for the 3D PES is

$$\begin{aligned} V = {} & 3V_{\text{atom}} + V(r_{12}) + V(r_{23}) + V(r_{31}) \\ & + \left(1 - s^2\right)\exp\left[-\alpha\left(\rho - \rho^{\Delta}\right)^2\right]g_l^{\Lambda}(\rho, s, \phi) \\ & + s^2\exp\left[-\alpha(\rho - \overline{\rho})^2\right]\overline{g}(\rho, s, \phi) \end{aligned} \tag{10}$$

where $V(r_{ij})$ is a two-body term expanded by the extended Rydberg function,

$$V(r_{ij}) = D_{\text{e}}\left(1 + \sum_{i=1}^{N} a_i\left(r_{ij} - r_{\text{e}}\right)^i\right)e^{-a_1\left(r_{ij} - r_{\text{e}}\right)} \ , \tag{11}$$

and the three-body terms are given by [14]

$$\begin{aligned} g_l^{\Lambda} = {} & \sum_{ijk} B_{ijk}\rho^i\left(s^2\right)^j\left(s^3\cos 3\phi\right)^k \\ & \pm s\sum_{ijk} C_{ijk}\rho^i\left(s^2\right)^j\left(s\cos 3\phi\right)^k \ , \end{aligned} \tag{12}$$

$$\overline{g} = \sum_{ijk} D_{ijk}\rho^i\left(s^2\right)^j\left(s^3\cos 3\phi\right)^k \ . \tag{13}$$

The upper sign in Eq. 12 is for the lower surface and the lower sign is for the upper surface. This functional form, in which the three-body terms are from Thompson et al [14], gives the correct analytical behavior even in the vicinity of the D_{3h} conical intersection, $D_{\infty h}$ collinear geometry, and the $Li + Li_2$ asymptotic region. Moreover, the analytical continuation from the lower surface to the upper one is satisfied automatically.

A vibrational analysis was performed at some critical points using the fitted PES by the Wilson FG analysis [20]. The F matrix was constructed by numerical differentiation of the analytical gradient.

The wavepacket calculations were performed by solving the time-dependent Schrödinger equation. The propagation in time was performed by the Chebychev expansion method [21] combined with the Newtonian interpolation technique [22]. The perimetric coordinates [23, 24] were used in our wavepacket calculation. These coordinates allow the Fourier method to be used for all

three modes. Transformation between coordinate and momentum space was performed by the 3D FFT method. The perimetric coordinates (z_1, z_2, z_3) are defined in relation to the three bond lengths (r_1, r_2, r_3) by

$$z_i = \left(-r_i + r_j + r_k\right), \quad r_i = \left(z_j + z_k\right)/2 \ . \tag{14}$$

For an X_3 system, that is, in which all the atoms are the same, the kinetic part of the Hamiltonian [22–24] is simply given by

$$K_V(z_1, z_2, z_3) = -\frac{h^2}{2}\left[\sum_{i=1}^{3}\left(v_{ii}\frac{\partial^2}{\partial z_i^2} + v_i\frac{\partial}{\partial z_i}\right) + \sum_{j>i=1}^{3} v_{ij}\frac{\partial^2}{\partial z_i \partial z_j}\right] \tag{15}$$

in the perimetric coordinates where

$$v_i = \frac{4}{\mu}\left(-\frac{1}{r_i} + \frac{1}{r_j} + \frac{1}{r_k}\right) \ , \tag{16}$$

$$v_{ii} = \frac{1}{\mu}\left(6 - b_{ij} - b_{ik} + b_{jk}\right) \ , \tag{17}$$

$$v_{ij} = \frac{1}{\mu}\left(2b_{ij} - 4\right) \ , \tag{18}$$

μ being the mass of the nucleus and b_{ij} given by

$$b_{ij} = \frac{r_i^2 + r_j^2 - r_k^2}{r_i r_j} \ . \tag{19}$$

The Jacobian of the perimetric coordinates is given by

$$\frac{1}{8}(z_1 + z_2)(z_2 + z_3)(z_3 + z_1) \ . \tag{20}$$

Classical trajectory calculations were performed to characterize the recurrences in the autocorrelation functions. The internal coordinates (r_1, r_2, θ) were adopted for solving Newton's equations and the Hamiltonian of the system was taken from the literature [25–27].

3 Potential energy surfaces

3.1 Potential energy curves of Li_2

The potential curves of Li_2 were calculated for the ground state, $X^1\Sigma_g^+$, and the low-lying singlet excited states, $A^1\Sigma_u^+$, $^1\Pi_g$, $^1\Pi_u$, and $2^1\Sigma_g^+$, which dissociate to $^2S + {}^2P$ in the atomic limit. Thirty-five points, calculated at an internuclear distance of 1.0–40.0 a.u., were fitted by an extended Rydberg function of order $N = 20$, and the spectroscopic constants were estimated by the Dunham method [28, 29]. The potential energy curves are depicted in Fig. 1 and the calculated spectroscopic constants are summarized in Table 1 together with the experimental values [30–32].

If we examine the results for the ground state, we see that for these MRCI calculations with state-specific CASSCF reference, as the quality of the basis set increases from VDZP, VTZP(*spd*), to VTZP(*spdf*), more accurate dissociation energies are obtained. The agreement between the VTZP (*spdf*) and experimental data is so good that we used these MRCI data for the fitting of the two-body terms in the Li_3 potential.

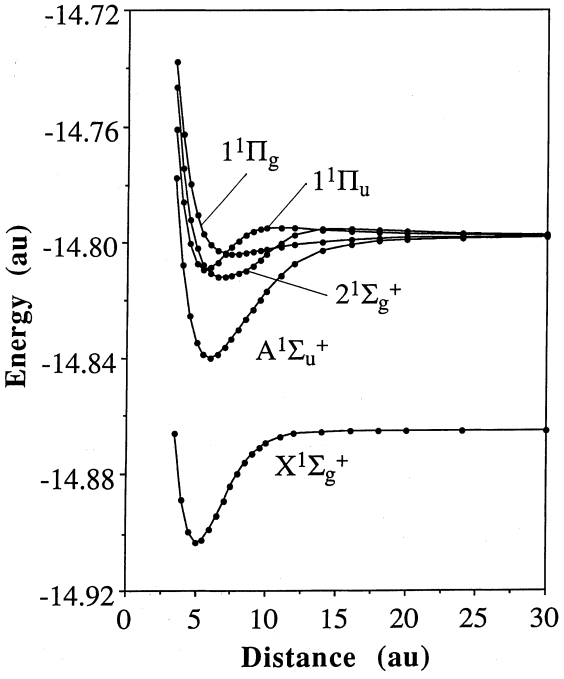

Fig. 1. Potential energy curves of the ground and low-lying singlet excited states of Li_2

The potential curves of the excited states were also calculated with the VTZP(*spdf*) basis set. Two types of CASSCF reference were examined; one was optimized by a state-averaged CASSCF for the five states and the other was optimized by a state-specific CASSCF. Since experimental results, where they exist, are not always consistent, it is not possible to say whether one or the other optimization method is better. For example the D_e of the $A^1\Sigma_u^+$ state was calculated as 9178.4 cm^{-1} and 9334.9 cm^{-1} with the state-averaged and state-specific optimizations respectively, while experimental values are 9469 cm^{-1} [31] and 8940 cm^{-1} [32]. Previous MCSCF work of Konowalow and Olson [33] predicted D_e to be 9299 cm^{-1}. For the $^1\Pi_u$ state, the state-specific R_e and ω_e values are in better agreement with the experimental values [30] than the state-averaged data. The $^1\Pi_u$ and $2^1\Sigma_g^+$ states have a hump in their potential curves. For the $^1\Pi_u$ state we calculated the inter nuclear separation at the hump and the potential barrier relative to the dissociation limit at 5.72 Å and 575 cm^{-1}.

3.2 Excited states of Li_3

Twelve low-lying electronic states of Li_3 were investigated for a C_{2v} structure. The CASSCF/MRCI potential energy curves of these states at $q_s = 3.2$ a.u. and $q_y = 0.0$ a.u. are depicted in Fig. 2. The equilibrium geometry, vertical and adiabatic excitation energies, and correspondence between the D_{3h} and C_{2v} representations are summarized in Table 2. The equilibrium geometry values (bond length and bond angle) were determined under the C_{2v} symmetry restriction and the MRCI

Table 1. CASSCF/MRCI Spectroscopic constants of Li_2

State	Basis set	Reference[a]	R_e [Å]	D_e [cm^{-1}]	ω_e [cm^{-1}]	$\omega_e\chi_e$ [cm^{-1}]	B_e [cm^{-1}]	α_e [cm^{-1}]
$X^1\Sigma_g^+$	VDZP	S-s	2.697	7922.3	340.0	2.48	0.662	0.006
	VTZP(*spd*)	S-s	2.685	8318.5	344.9	2.45	0.668	0.007
	VTZP(*spdf*)	S-s	2.667	8530.4	345.1	2.27	0.677	0.007
Exptl.			2.673[b]	8541[b]	351.4[b]	2.58[b]	0.672[c]	0.007[c]
$A^1\Sigma_u^+$	VTZP(*spdf*)	S-a	3.143	9178.4	252.1	1.51	0.487	0.005
	VTZP(*spdf*)	S-s	3.103	9334.9	253.1	1.91	0.500	0.007
Exptl.			3.108[b]	8940[b] 9469[d]	255.4[b]	1.58[b]	0.498[c]	0.005[c]
$1^1\Pi_g$	VTZP(*spdf*)	S-a	4.093	1347.1	93.5	1.80	0.288	0.009
	VTZP(*spdf*)	S-s	4.042	1416.4	94.5	1.41	0.295	0.009
$1^1\Pi_u$	VTZP(*spdf*)	S-a	2.968	2626.9	269.1	3.10	0.547	0.008
	VTZP(*spdf*)	S-s	2.935	2754.1	268.4	2.56	0.559	0.008
Exptl.			2.935[c]	...	270.1[c]	2.67[c]	0.558[c]	0.009[c]
$2^1\Sigma_g^+$	VTZP(*spdf*)	S-a	3.638	3236.7	145.6	1.47	0.364	0.005

[a] "S-s" and "S-a" denote the state-specific and state-averaged CASSCF references, respectively
[b] Ref. [32]
[c] Ref. [30]
[d] Ref. [31]

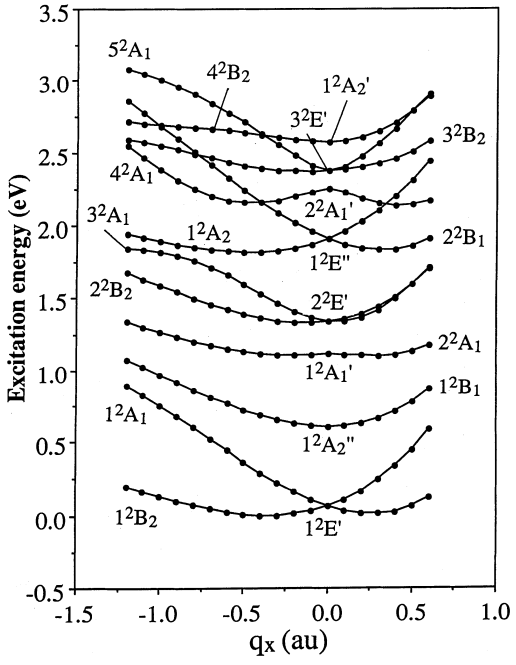

Fig. 2. Potential energy curves of the ground and low-lying excited states of Li_3 for $q_s = 3.2$ a.u. and $q_y = 0.0$ a.u

calculations were performed at q_s = 2.8–4.0 a.u. and $q_x = -1.2$–0.6 a.u. with an interval of 0.1 a.u. The shapes of the calculated potential energy curves differ between the MRCI and CASSCF calculations, especially for the 2^2A_1 state. The $4^2E'$ and $2^2E''$ states lie above the 12 low-lying states and may be important as intermediate states for SEP experiments.

So far, only the vertical excitations of Li_3 have been investigated, by an MRD-CI calculation [15]. The ordering of the vertical excitations found here is identical to that in Ref. 15 up to the 3^2B_2 state, although the 4^2A_1 state is missing. Our values for the vertical excitation energies are almost the same as the estimated full-CI values of Ref. [15]. In another study, a vibrational progression was observed at 1.81 eV above the ground state and identified as the $2^2E'$ state [16]. Here, we find the $2^2E'$ and $1^2E''$ states around this energy region, with ΔE = 1.3 and 1.8 eV, respectively.

The electronic structure of Li_3 is analogous to that of Na_3, and therefore, the ordering of the excited states and the shapes of the PESs can be assumed to be similar. A generalized valence-bond/MRCI study by Cocchini et al was reported for the 2D PESs of the Na_3 excited states [2] Our excitation energies of Li_3 are larger than those of Na_3. A remarkable difference between our PESs for Li_3 and those found for Na_3 is the interaction of the $1^2A_1'$ and $2^2E'$ states. The degenerate pair of the $2^2E'$ state consists of the 2^2B_2 and 3^2A_1 states for Li_3 and the 2^2B_2 and 2^2A_1 states for Na_3 [2]. This pair and the $3^2E'$ state do not show a conical intersection. The double minima of the 2^2A_1 state of Li_3 are quite shallow at $q_s = 3.2$ a.u. The cross-sections of other excited states of Li_3 obtained in the present study show behavior similar to those of Na_3, and therefore, the equilibrium geometry values of the excited states show similar trends. The 1^2B_1, 1^2A_1, and 5^2A_1 states are stable for an equilateral triangle geometry, while the equilibrium geometry of the other states is an isosceles triangle. The 4^2B_2 state is dissociative, the same as for Na_3. The optimized q_s of the $1^2A_2''$ state is small, 3.0 a.u., which shows that the molecul shrinks in comparison with the ground state.

3.3 3D PES of Li_3 and fitting

The two lowest adiabatic 3D PESs of Li_3 were calculated by the state-averaged CASSCF/MRCI method with a VTZP(*spdf*) basis set. Figure 3 displays the cross-sections of the lower surface at (a) $q_s = 3.2$ a.u. and (b) $q_x = 0.0$ a.u. The 3D plots of the lower and upper surfaces at $q_s = 3.2$ a.u. are depicted in Fig. 4. These adiabatic surfaces correlate with the 1^2A_1 and 1^2B_2 states in C_{2v} and the degenerate $1^2E'$ state in D_{3h}. The

Table 2. Parameters of excited states of Li_3 calculated by the CASSCF/MRCI method with VTZP(*spd*)

State		Equilibrium geometry[a]				Excitation energy [eV]	
D_{3h}	C_{2v}	Bond length [Å][b]	Bond angle [deg]	q_s [au]	q_x [au]	Vertical	Adiabatic
$1^2E'$[c]	1^2B_2	2.79	71.8	3.21	−0.362	...	...
	1^2A_1	3.06	52.0	3.19	0.269	0.26	0.01
$1^2A_2''$	1^2B_1	2.75	60	3.0	0.0	0.67	0.56
$1^2A_1'$	2^2A_1	3.22	49	3.3	0.4	1.11	1.09
$2^2E'$	2^2B_2	3.03	66	3.4	−0.2	1.34	1.28
	3^2A_1	3.12	60	3.4	0.0	1.50	1.29
$1^2E''$	1^2A_2	2.88	79	3.4	−0.6	1.82	1.80
	2^2B_1	3.22	49	3.3	0.4	2.13	1.82
$2^2A_1'$	4^2A_1	3.61	45	3.6	0.6	2.15	2.01
$3^2E'$	3^2B_2	3.26	68	3.7	−0.3	2.38	2.26
	5^2A_1	3.3	60	3.6	0.0	2.55	2.27
$1^2A_2'$	4^2B_2	Dissociative				2.61	2.44

[a] Equilibrium geometry is determined under the C_{2v} symmetry restriction
[b] Bond length of the equal sides of the isosceles triangle
[c] The lowest two adiabatic states are optimized with VTZP(*spdf*)

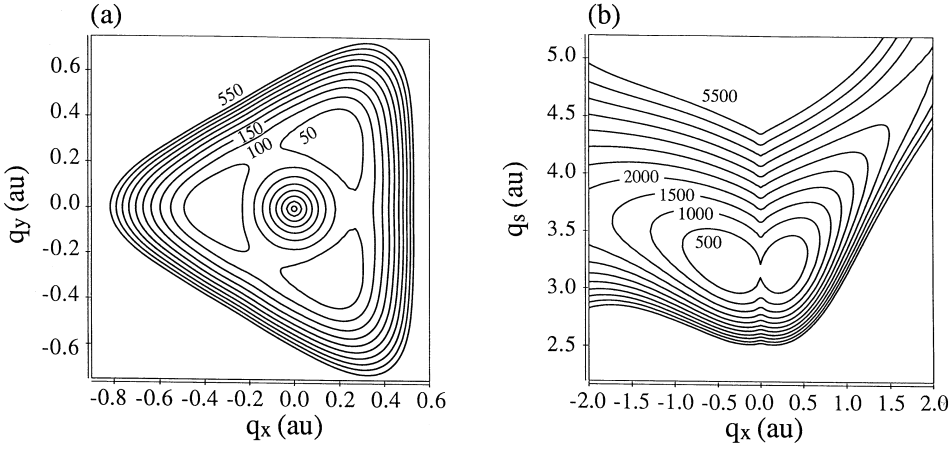

Fig. 3a,b. Cross-sections of the lower adiabatic surface of Li_3 at **a** $q_s = 3.2$ a.u. and **b** $q_y = 0.0$ a.u. Energies are given relative to the C_{2v} obtuse geometry in cm^{-1}

calculated lower surface represents the characteristics of the PESs of the alkali trimer: the shallow three-fold wells (C_{2v} obtuse), barriers to pseudorotation (C_{2v} acute), and conical intersection (D_{3h}), which are shown in Fig. 3a and Fig. 4. The potential seam is clearly found at $q_y = 0$ in Fig. 3b.

Table 3 summarizes the total energy, interaction energy, and relative energy of the critical points with their geometries. From this data we see that the C_{2v} obtuse configuration is the lowest in energy, followed by C_{2v} acute, D_{3h}, and $D_{\infty h}$. These energies were then compared to the total energy of the $Li + Li_2$ asymptotic structure, calculated at −22.335836 a.u. to derive the interaction energies, in the third column of Table 3.

We next derived the harmonic frequencies using the fitted PES (even though the harmonic approximation is not quantitatively valid for an X_3-type system [34]) shown at the right in Table 3. Note that the C_{2v} acute geometry has an imaginary frequency of 210 cm^{-1} for the asymmetric stretch and the energy gradient does not vanish at the $D_{\infty h}$ collinear structure.

The lower surface was fitted by the self consistent analytical function of Eq. 10. Expansion coefficients of the two- and three-body terms were determined by a least squares fit with equal weighing for all the points and variation of the nonlinear terms. The ρ^{Δ} and $\overline{\rho}$ values were determined as 3.2330 and 4.4662 a.u., respectively, according to the optimized C_{2v} obtuse and $D_{\infty h}$ collinear structures. Optimized expansion coefficients of the two-body terms, a_i, and three-body terms [14], B_{iJk}, C_{iJk}, and D_{iJk}, are listed in Table 4. Here the indices i, j, and k represent the exponents of ρ, s, and ϕ, respectively, as in Eqs. 12 and 13, and J gives the total exponent s, namely, $J = 2j + 3k$ for B-type and D-type terms and $J = 2j + k + 1$ for a C-type term [14]. The root mean square (rms) errors of the fitting are summarized in Table 5 for those energy thresholds which determined the energy data to be fitted.

For the two-body terms, the fitting was performed with 31 points from 1.5 to 40.0 a.u. for the Li_2 ground state calculated by the CASSCF/MRCI method using the VTZP(*spdf*) basis set. The rms error for the fitting of

the two-body terms is 2.47 cm^{-1}. The total energy of the three Li atoms, $3E_{atom} = -22.2981117$ a.u., was determined for the equilateral triangle geometry of Li_3 at $R = 20.0$ a.u.

An analytical fit of the 3D PES was performed only for the lower adiabatic surface. The CASSCF/MRCI calculations were performed at the four representative geometries: (a) 527 points in the neighborhood of the equilateral triangles, $q_s = 2.85$–4.45 a.u., $q_x = -1.4$–0.7 a.u., and $q_y = 0.0$–1.0 a.u.; (b) 153 points in the $Li + Li_2$ asymptotic region, $r_1 = r_2 = 7.0$–30.0 a.u., $r_3 = 4.5$–6.5 a.u. and $r_1 = 5.0$, $r_2 = 7.0$–30.0 a.u., $\theta = 50°$–$180°$; (c) 22 points for the $D_{\infty h}$ collinear geometry, $r_1 = r_2 = 4.5$–6.5 a.u.; (d) 72 points around the conical intersection, $q_s = 2.8$–4.4 a.u., $q_x^2 + q_y^2 \leq 0.15^2$. Final parameters were determined with those 680 points (out of 774), whose total energy was less than −22.335 a.u.

The analytical continuation of the fitted function to the upper surface was examined. The total energies of the upper surface calculated by the MRCI method were compared to those estimated by the fitted PES around the D_{3h} conical intersection. The rms errors of the deviation from the MRCI calculation are summarized in Table 5. Though the data of the upper surface were not included in the least squares fit, the rms error is as small as 45.2 cm^{-1} for the energy data up to −22.340 a.u. This shows that the present fitted PES satisfies the analytical continuation around the D_{3h} conical intersection region.

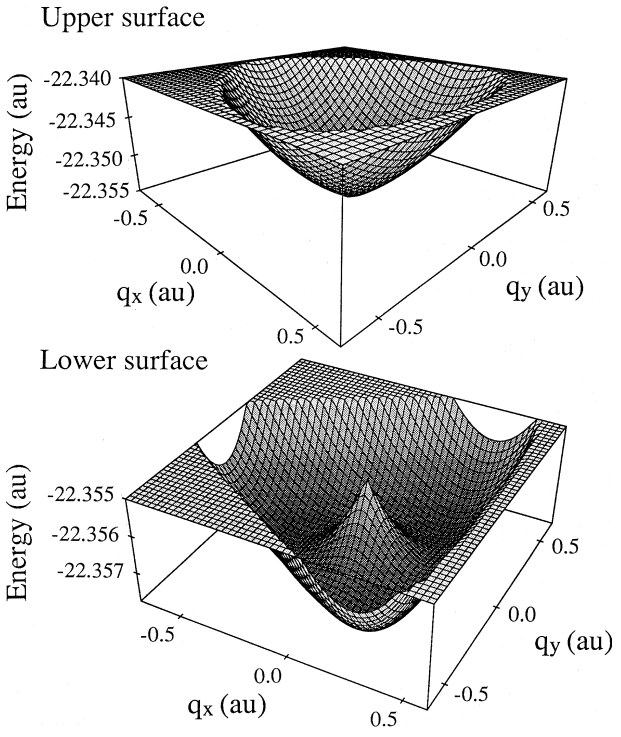

Fig. 4. Three-dimensional plots of the lower and upper surfaces of Li_3 at $q_s = 3.2$ a.u.

4 3D wavepacket dynamics

The vibrational motion and the pseudorotation of Li_3 were investigated by the time-dependent wavepacket formalism using the 3D PES described in Sect. 3.3. Vibronic coupling was not considered and the wavepackets were propagated in the lower surface. Perimetric coordinates were used in the wavepacket calculations, while the analysis was undertaken in D_{3h} symmetry coordinates to better visualize the nuclear motion. The 32 grid points from 1.0 a.u. to 11.85 a.u. with a grid spacing of 0.35 a.u. were adopted for each direction of the perimetric coordinates. The density of the wavepacket was analyzed by projecting it onto the $q_x q_y$ plane.

First, the vibrational ground state of Li_3 was calculated by an arbitrary wave function being propagated in imaginary time. The density of the converged wave function projected onto the $q_x q_y$ plane is shown in Fig. 5. The density is delocalized over the three-fold wells of the C_{2v} obtuse structure, since the barriers of the pseudorotation are low, about 70 cm^{-1}. However, it still reflects the shape of the PES. The vibronic ground state of Li_3 calculated by Gerber and Schumacher [12] also shows this delocalization.

Real time wavepacket propagations were performed for simulation of a SEP experiment and the autocorrelation functions were calculated to find the recurrences. In the SEP spectrum of Na_3 [4], the electronically excited C state was taken as an intermediate state (the $2^2E''$ state in D_{3h}). Because the PESs of the A (1^2E) and C states resemble each other in the C_{2v} cut of Na_3[2]), it is of interest to perform simulations based on the A state. Since the 3D PES of the A state was not calculated, we adopted a 3D distribution of the initial wavepacket similar to that of the vibrational ground state of the adiabatic electronic ground state. One of the three-fold minima of the A state was calculated as (3.4, −0.6, 0.0) in

Table 3. Energy, equilibrium geometry, and frequency at the critical points of the lowest surface for Li_3 calculated by the CASSCF/MRCI method with VTZP(*spdf*)

Structure	Total energy [au]	Interaction energy [kcal/mol]	Relative energy [cm^{-1}]	Equilibrium geometry			Frequency [cm^{-1}][a]		
				$R_1 = R_2$ [a.u.]	R_3 [a.u.]	Angle [deg]	ss	as	b
C_{2v} obtuse	−22.357 736	13.73	0	5.28	6.19	71.8	325	175	186
C_{2v} acute	−22.357 401	13.52	74	5.78	5.07	52.0	337	210i	246
D_{3h}	−22.355 430	12.28	506	5.47	10.94	180.0	...	...	...
$D_{\infty h}$	−22.346 693	5.55	2423	5.48	5.48	60.0	...	...	...

[a] ss: symmetric stretch; as: asymmetric stretch; b: bend

Table 4. Optimized parameters of the 3D Li_3 PES. ($3E_{atom} = -22.2981117$ a.u.)

Two-body terms		Three-body terms											
	$r_0 = 5.035$	$\alpha = 0.0355256$				$\rho^{\Delta} = 3.2330$				$\overline{\rho} = 4.4662$			
		B^a_{iJk}				C^b_{iJk}				D^a_{iJk}			
		i	J	k		i	J	k		i	J	k	
a_1	0.1000000D+01	0	0	0	0.6284778D−01	0	1	0	0.6019228D−01	0	0	0	−0.2098829D+03
a_2	−0.1299838D+00	1	0	0	0.4873348D−01	1	1	0	−0.5829509D−01	1	0	0	−0.3443810D+02
a_3	0.1021043D−01	2	0	0	−0.2401367D−01	2	1	0	0.1318383D−01	2	0	0	0.5025022D+00
a_4	−0.3040201D−02	3	0	0	0.2484766D−02	3	1	0	−0.9829767D−03	3	0	0	−0.2055845D−01
a_5	−0.6868411D−03	0	2	0	0.1484827D+03	0	2	1	−0.3752211D+00	0	2	0	0.2092736D+03
a_6	0.8650762D−03	1	2	0	0.3906214D+02	1	2	1	0.2793771D+00	1	2	0	0.3496965D+02
a_7	−0.1426472D−03	2	2	0	0.1892065D+01	2	2	1	−0.6868779D−01	2	2	0	−0.6374238D+00
a_8	−0.2998075D−04	3	2	0	0.1638344D+00	3	2	1	0.5472993D−02	3	2	0	0.3129364D−01
a_9	0.1527399D−04	0	3	1	−0.3620238D+00	0	3	0	0.5314571D+00	0	3	1	−0.1268602D+01
a_{10}	−0.2741980D−05	1	3	1	0.3360201D+00	1	3	0	−0.4275517D+00	1	3	1	0.6415711D+00
a_{11}	0.2748785D−06	2	3	1	−0.9780367D−01	2	3	0	0.1056152D+00	2	3	1	−0.9231878D−01
a_{12}	−0.1590390D−07	3	3	1	0.9124755D−02	3	3	0	−0.8391936D−02	3	3	1	0.2620158D−02
a_{13}	0.4070483D−09	0	4	0	0.1337743D+01	0	3	2	0.2241320D+00	0	4	0	0.8566161D+00
a_{14}	0.9815995D−11	1	4	0	−0.1012053D+01	1	3	2	−0.1689858D+00	1	4	0	−0.6239938D+00
a_{15}	−0.1180322D−11	2	4	0	0.2375527D+00	2	3	2	0.4108432D−01	2	4	0	0.1464640D+00
a_{16}	0.4022074D−13	3	4	0	−0.1778945D−01	3	3	2	−0.3202865D−02	3	4	0	−0.1121198D−01
a_{17}	−0.5385719D−15	0	5	1	−0.1140902D+02	0	4	1	−0.1522661D+01	0	5	1	0.1216768D+01
a_{18}	−0.3073918D−17	1	5	1	0.7594613D+01	1	4	1	0.8678965D+00	1	5	1	−0.6087692D+00
a_{19}	0.1737894D−18	2	5	1	−0.1677874D+01	2	4	1	−0.1705241D+00	2	5	1	0.8467807D−01
a_{20}	−0.1470184D−20	3	5	1	0.1221622D+00	3	4	1	0.1150517D−01	3	5	1	−0.2045147D−02
						0	4	3	0.1404559D+02				
						1	4	3	−0.8644884D+01				
						2	4	3	0.1743932D+01				
						3	4	3	−0.1136243D+00				

[a] $J = 2j + 3k$
[b] $J = 2j + k + 1$

Table 5. Root mean square (rms) errors and numbers of fitted and examined points

	Lower surface			Upper surface		
	Energy threshold [a.u.]	Number of fitted points	rms error [cm^{-1}]	Energy threshold [a.u.]	Number of examined points	rms error [cm^{-1}]
Fit 1	−22.335	680	8.26	−22.340	134	45.2
				−22.345	102	26.3
				−22.350	36	16.6
Fit 2	−22.336	581	3.79			
Fit 3	−22.340	475	2.34			

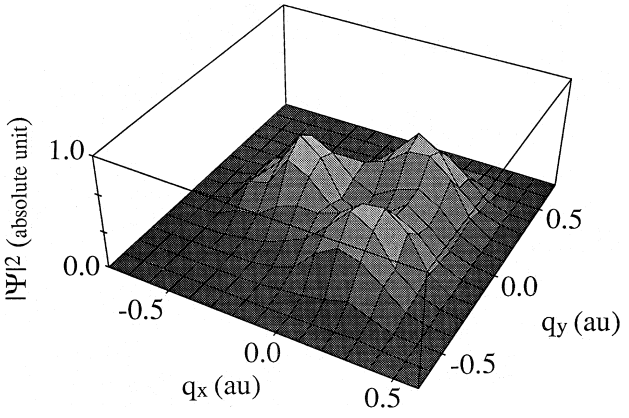

Fig. 5. Density of the vibrational ground state of Li_3 projected onto the q_xq_y plane

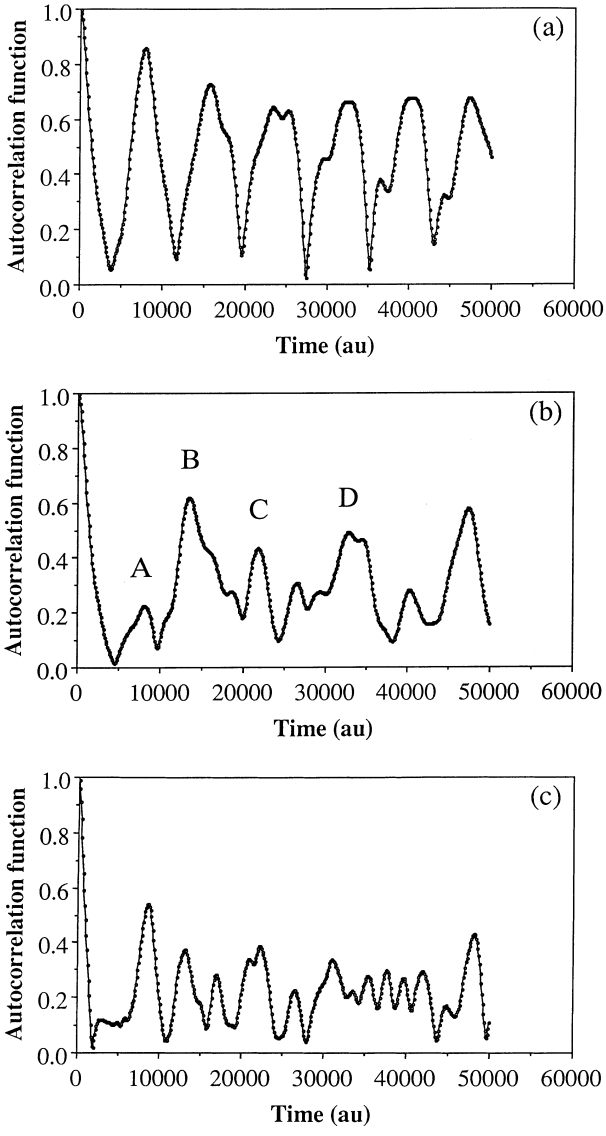

Fig. 6a–c. Autocorrelation functions calculated by 3D wavepacket propagation. Initial wavepackets are 3D-gaussian centered at **a** case 1 $(q_s, q_x, q_y) = (3.4, -0.6, 0.0)$ and $(3.4, 0.3, \pm 0.6/\sqrt{3})$, **b** case 2 $(q_s, q_x, q_y) = (3.4, -0.6, 0.0)$, and **c** case 3 $(q_s, q_x, q_y) = (3.21, -0.8, 0.0)$ and $(3.21, 0.4, \pm 0.8/\sqrt{3})$. The assignments of peaks A, B, C, D will be discussed in conjunction with Fig. 8

the (q_s, q_x, q_y) representation, which is different from the ground state (3.21, −0.36, 0.0). Three cases of initial conditions which reflect the stable geometry of the A state were examined. In case 1, the pseudorotation barriers of the A state were low, as in the ground state; therefore, a three-centered 3D-gaussian wavepacket whose centers were at (3.4, −0.6, 0.0) and $(3.4, 0.3, \pm 0.6/\sqrt{3})$ was adopted to represent the delocalized wave function. This condition is different from the situation in Na_3 dynamics [7]. The autocorrelation function calculated for case 1 is shown in Fig. 6a and the projected density of the wavepacket during the propagation is shown in Fig. 7. In case 2 (Fig. 6b), to enable direct comparisons a one-center 3D-gaussian was adopted for the initial condition, as was done for Na_3 [7]. In case 3 (Fig. 6c), a three-centered 3D-gaussian with centers at $(3.21, -0.8, 0.0)$ and $(3.21, 0.4, \pm 0.8/\sqrt{3})$ was used to represent the distorted molecular structure. The energy expectation value $\langle E \rangle$ for cases 1 and 2 is 610 cm^{-1} and that for case 3 is 920 cm^{-1}.

The recurrences of the autocorrelation function for case 1 are simple and large, while those for case 2 are rather complex, as seen in Fig. 6. The fine structure of the recurrences is obvious in case 2. In both cases, the recurrences occur at time T = 8,000, ~15,000, ~23,000, and ~33,000 a.u. The relationship between these recurrences and the motions of the wavepacket is clearly shown by projecting the density of the wavepacket onto the q_xq_y plane. Figure 7 displays the time-evolution of wavepacket density for the first recurrence of case 1. The wavepacket moves to the D_{3h} region at $T = 4000$ a.u. and then comes back to the initial position. The autocorrelation function of case 3 (Fig. 6c) becomes more complex, though the recurrence times are almost the

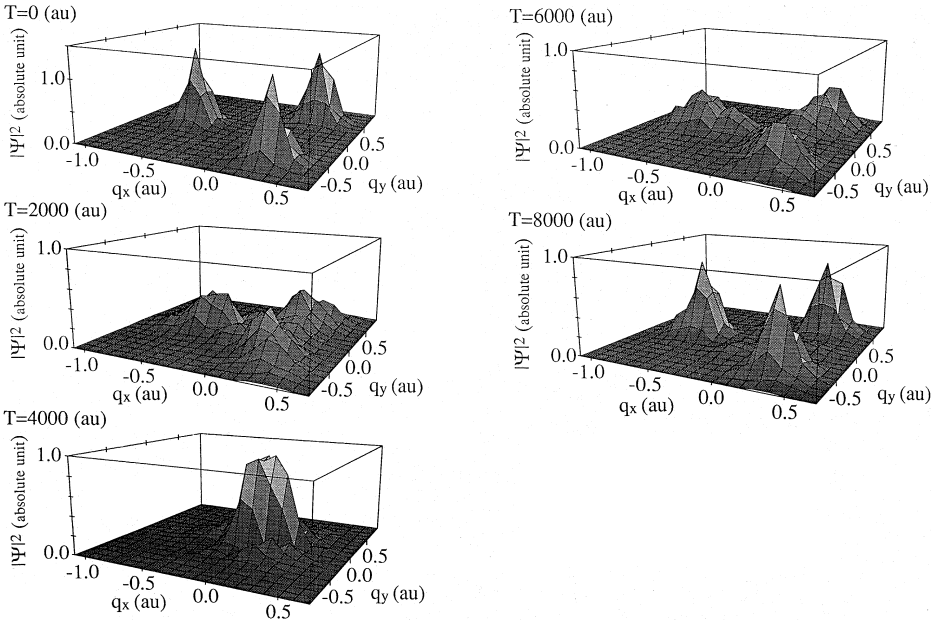

Fig. 7. Wavepacket density during propagation, projected onto the $q_x q_y$ plane

same as in the preceding two cases. The recurrences in the autocorrelation functions of Li_3 are large in comparison with those of Na_3 [4,5]. This is because the pseudorotation is essential in Li_3 and the barriers are very low.

5 Classical trajectory analysis

Next, classical trajectory calculations were performed to characterize the recurrences of the autocorrelation functions. Some representative trajectories taken for the autocorrelation function data of case 2 (Fig. 6b) are shown in Fig. 8, projected onto the $q_x q_y$ plane. Recurrence A (Fig. 6b) is assigned to the motion of the trajectories that are localized in the single well of the C_{2v} obtuse geometry (Fig. 8a). The trajectories shown in Fig. 8b, which represent the pseudorotation of Li_3, are attributed to recurrence B (Fig. 6b) with the second recurrence of the trajectory type seen in (Fig. 8a). Recurrence C of Fig. 6b includes the motion shown in Fig. 8c, which goes around the D_{3h} conical intersection, and also that in Fig. 8d. Various trajectories such as those in Fig. 8e are attributed to the fourth recurrence D in Fig. 6b. If the initial wavepacket delocalizes over all the three-fold wells as in case 1, all of these trajectories contribute to all the recurrences. This is the reason for the large recurrences of the case 1 wavepacket dynamics.

Finally, the autocorrelation functions were simulated using a classical trajectory approach. The wavepacket dynamics were described by the sum of the classical trajectories. The initial 3D-gaussian of the wavepacket was described by 9,310 points for which the weight of the gaussian distribution and the autocorrelation is calculated by the overlap between the initial 3D-gaussian and the gaussian function on the trajectory points. The conditions of cases 1 and 2 were imposed. The autocorrelation functions thus calculated by the sum of the trajectories are depicted in Fig. 9. The relative intensity and the interval of the recurrence are well simulated for early recurrences. The deviation in the long-time region may be due to the fact that the discretization of the phase space by the present trajectory points is not adequate and the spread of the phase space of each trajectory is not included.

6 Summary

The ground and excited electronic states of Li_3 and the vibrational motion and pseudorotation in the ground state have been investigated. The 3D PES of the adiabatic ground state was calculated by the CASSCF/MRCI method and fitted by a consistent analytical function. The 12 low-lying electronic states of Li_3 were investigated in the C_{2v} structure and the vertical and adiabatic excitation energies were calculated.

The 3D wavepacket dynamics formalism was used for simulations of a SEP experiment in which the A state was taken as an intermediate. The recurrences in the autocorrelation function of Li_3 were large in comparison to those of Na_3 due to the low barriers to pseudorotation. The recurrences in the autocorrelation functions were characterized by classical trajectory calculations and the accumulation of the trajectories simulated well the quantum-mechanical autocorrelation function in the short-time region. Each regular motion inserted into a chaotic trajectory is itself a short-lived species, which exhibits an important feature of dynamics at transition state regions.

Acknowledgements. The authors acknowledge the late Professor K. Fukui for valuable discussions and encouragement. M.E. is grateful to the Japan Society for the Promotion of Science for a research fellowship. K.Y. thanks the Sumitomo Foundation for support. The present work is partially supported by a Grant-in-Aid for Scientific Research from the Japanese Ministry of Education, Science, and Culture.

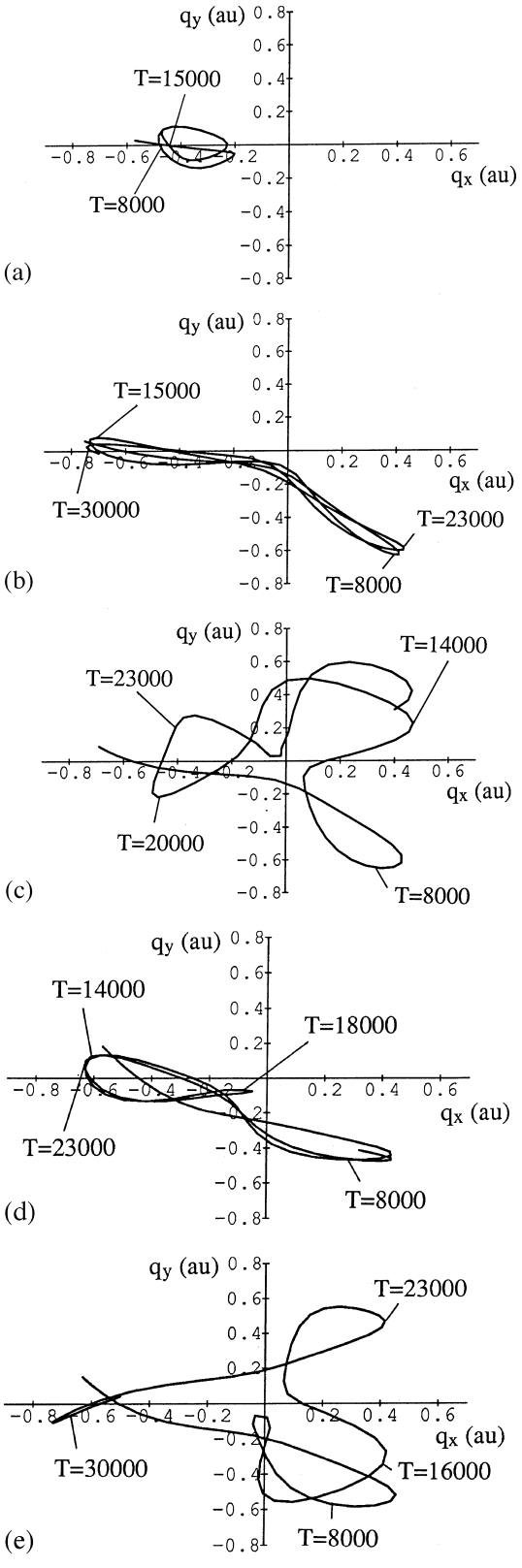

Fig. 8a–e. Representative classical trajectories in the $q_x q_y$ plane for recurrences of the autocorrelation functions

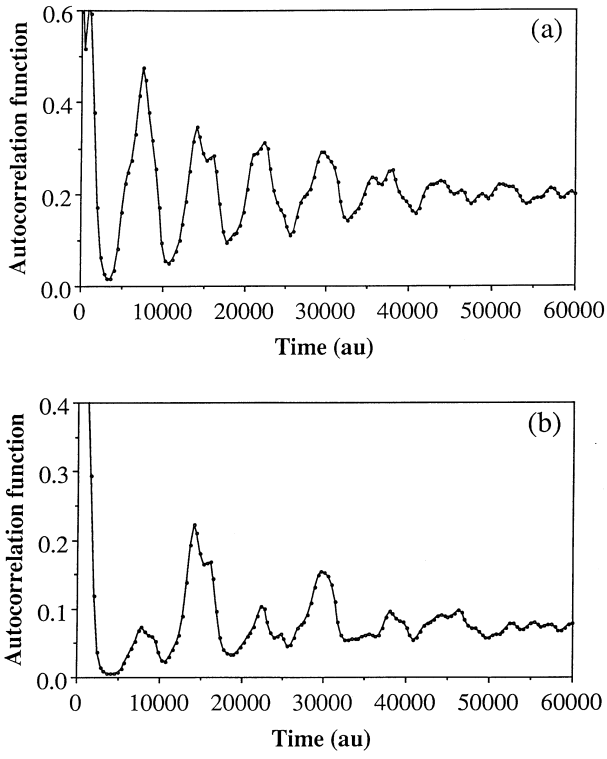

Fig. 9a,b. Autocorrelation functions calculated by the 9315 classical trajectories. These simulations correspond to the wavepacket dynamics with the initial wavepacket centered at **a** case 1 $(q_s, q_x, q_y) = (3.4, -0.6, 0.0)$ and $(3.4, 0.3, \pm 0.6/\sqrt{3})$ and **b** case 2 $(q_s, q_x, q_y) = (3.4, -0.6, 0.0)$

References

1. Delacretaz G, Grant ER, Whetten R, Wöste L, Zwanziger JW (1986) Phys Rev Lett 56:2598
2. Cocchini F, Upton TH, Andreoni W (1988) J Chem Phys 88:6068
3. Meiswinkel R, Köppel H (1990) Chem Phys 144:117
4. Broyer M, Delacretaz G, Ni G-Q, Whetten RL, Wolf J-P, Wöste L (1989) J Chem Phys 90:843; (1989) Phys Rev Lett 62:2100
5. Llorente JMG, Taylor HS (1989) J Chem Phys 91:953; Taylor HS (1989) Acc Chem Res 22:263
6. Morais VMF, Varandas AJC (1992) J Phys Chem 96:5704
7. Gaus J, Kobe K, Bonacic-Koutecky V, Kühling H, Manz J, Reischl B, Rutz S, Schreiber E, Wöste L (1993) J Phys Chem 97:12509; de Vivie-Riedle R, Gaus J, Bonacic-Koutecky V, Manz J, Reischl B, Rutz S, Schreiber E, Wöste L (1996) Femtochemistry – ultrafast chemical and physical processes in molecular systems. World Scientific, Singapore; Reischl B, de Vivie-Riedle R, Runz S, Schreiber E (1996) J Chem Phys 104:8857
8. Baumert T, Thalweiser R, Gerber G (1993) Chem Phys Lett 209:29; Baumert T, Gerber G (1995) Adv Atom Mol Opt Phys 35:163
9. Schön J, Köppel H (1994) Chem Phys Lett 231:55; (1995) J Chem Phys 103:9292
10. Dobbyn AJ, Hutson JM (1994) J Phys Chem 98:11428; (1995) Chem Phys Lett 236:547
11. Reischl B (1995) Chem Phys Lett 239:173
12. Gerber WH, Schumacher E (1978) J Chem Phys 69:1692
13. Martins JL, Car R, Buttet J (1983) J Chem Phys 78:5649
14. Thompson TC, Izmirlian G Jr, Lemon SL, Truhlar DG, Mead CA (1985) J Chem Phys 82:5597
15. Beckmann H-O (1982) Chem Phys Lett 93:240

16. Wolf J-P, Delacretaz G, Wöste L (1989) Phys Rev Lett 63:1946
17. Werner H-J, Knowles PJ (1988) J Chem Phys 89:5803; (1988) Chem Phys Lett 145:514; (1992) Theor Chim Acta 84:95
18. MOLPRO is a package of ab initio programs written by Werner HJ and Knowles PJ, with contributions from Almlof J, Amos RD, Deegan MJO, Elbert ST, Hampel C, Meyer W, Peterson K, Pitzer R, Stone AJ, Taylor PR
19. Dunning TH (1989) J Chem Phys 90:1007
20. Wilson EB Jr, Decius JC, Cross PC (1955) Molecular vibration Dover, New York
21. Tal-Ezer H, Kosloff R (1984) J Chem Phys 81:3967; Kosloff R, Tal-Ezer H (1986) Chem Phys Lett 127:223
22. Kosloff R (1988) J Phys Chem 92:2087; (1992) Time-dependent quantum molecular dynamics. Plenum, New York; (1994) Annu Rev Phys Chem 45:145
23. Pekeris CL (1958) Phys Rev A 112:1649
24. Sutcliffe BT (1992) Mol. Phys 75:1233; Sutcliffe BT, Tennyson J (1991) Int J Quantum Chem 39:183
25. Cross PC, Van Vleck JH (1933) J Chem Phys 1:350
26. Blais NC, Bunker DL (1962) J Chem Phys 37:2713
27. Bunker DL (1962) J Chem Phys 37:393
28. Dunham JL (1932) Phys Rev 41:713, 721
29. Hulburt HM, Hirschfelder JO (1941) J Chem Phys 9:61
30. Herzberg G (1960) Spectra of diatomic molecules. Van Nostrand, New York
31. Hsu DK (1975) Ph.D. dissertation, Fordham University
32. Kusch P, Hessel MM (1977) J Chem Phys 67:586
33. Konowalow DD, Olson ML (1979) J Chem Phys 71:450
34. Thompson TC, Truhlar DG, Mead CA (1985) J Chem Phys 82:2392